

Scalable method for Bayesian experimental design without integrating over posterior distribution

Vinh Hoang^{1*}, Luis Espath², Sebastian Krumscheid³, and Raúl Tempone^{1,4}

¹Chair of Mathematics for Uncertainty Quantification, RWTH Aachen University
Germany.

²Faculty of Science, University of Nottingham, United Kingdom.

³Steinbuch Center for Computing and Institute for Applied and Numerical
Mathematics, Karlsruhe Institute of Technology, 76131 Karlsruhe, Germany.

⁴Computer, Electrical and Mathematical Sciences and Engineering, KAUST, and
Alexander von Humboldt professor in Mathematics of Uncertainty Quantification,
RWTH Aachen University.

*Corresponding author: hoang@uq.rwth-aachen.de

July 3, 2023

Abstract

We address the computational efficiency in solving the A-optimal Bayesian design of experiments problems for which the observational model is based on partial differential equations and, consequently, is computationally expensive to evaluate. A-optimality is a widely used and easy-to-interpret criterion for the Bayesian design of experiments. The criterion seeks the optimal experiment design by minimizing the expected conditional variance, also known as the expected posterior variance. This work presents a novel likelihood-free method for seeking the A-optimal design of experiments without sampling or integrating the Bayesian posterior distribution. Our proposed approach is developed based on two properties of the conditional expectation: the law of total variance and the orthogonal projection property. The expected conditional variance can be obtained via the variance of the conditional expectation using the law of total variance, while we take advantage of the orthogonal projection property to approximate the conditional expectation. Through an asymptotic error estimation, we show that the intractability of the posterior does not affect the performance of our approach. We use an artificial neural network (ANN) to approximate the nonlinear conditional expectation to implement our method. For dealing with continuous experimental design parameters, we integrate the training process of the ANN into minimizing the expected conditional variance. Specifically, we propose a non-local approximation of the conditional expectation and apply transfer learning to reduce the number of evaluations of the observation model. Through numerical experiments, we demonstrate that our method significantly reduces the number of observational model evaluations compared with common importance sampling-based approaches. This reduction is crucial, considering the computationally expensive nature of these models.

Contents

1	Introduction	2
2	Background	4
3	Estimation of the tECV using PACE	6
3.1	PACE-based MC estimator of the tECV	6
3.2	Estimation of errors	8
3.3	Reduced variance estimator	9
4	Numerical experiment: linear-gaussian setting	10
4.1	One-dimensional case	10
4.2	High-dimensional case	11
5	Stochastic optimization for the continuous design domain	12
5.1	Non-local approximation of the conditional expectation	13
5.2	Algorithm	14
6	Numerical experiment: Electrical impedance tomography	16
6.1	Formulation and finite element model of EIT experiment	16
6.2	Numerical results	17
6.2.1	Error analysis in estimating the tECV	18
6.2.2	Minimization of the tECV	19
7	Conclusion	20
A	Computing tECV using the IS approach	21
B	Proofs	22
B.1	Proof of Proposition 1	22
B.2	Proof of Proposition 2	22
B.3	Orthogonality property of the CE	23
C	Linear approximation of the CE	24
C.1	Analytical formulation of the linear approximation	24
C.2	Empirical linear approximation of the CE	25
D	Reduced variance estimators of MSE and tECV	25
E	Gradient of the weighted MSE w.r.t. design parameters	26
F	Derivation of the finite element formulation	26

1 Introduction

The design of experiments (DOE) aims to systematically plan experiments for collecting data and making accurate conclusions about a particular process or system. Applications of this methodology are wide-ranging such as in engineering [1, 2], pharmaceutical [3, 4], and biology [5, 6]. Fundamentally, ill-posedness and uncertainty naturally arise in the DOE. Bayesian DOE provides

a general probabilistic framework to deal with these challenges [7, 8]. There are several optimal criteria in the Bayesian DOE framework, for example, the A-optimal criterion minimizes the expected conditional variance (ECV), whereas the information gain criterion maximizes the expected Kullback-Leibler divergences between prior and posterior distributions. This paper focuses on the first criterion, *i.e.*, the A-optimal design of experiments (A-optimal DOE). Compared with alternative optimality criteria, the A-optimal criterion is of significantly practical appeal due to its straightforward interpretation and visualization of the posterior variance. Indeed, a reduced posterior variance indicates the reduction of uncertainty.

Dealing with the Bayesian DOE generally requires estimating the expected conditional statistical quantities, such as the expected conditional variance or the expected information gain. Because this task is significantly computational expensive, many previous works aimed to develop efficient methods to perform it. Alexanderian et al. [9] proposed a scalable method for solving the A-optimal DOE problem, specifically tailored on scenarios where the observational map is linear. For the nonlinear case, the posterior is typically intractable. Although the Markov Chain Monte Carlo algorithm or the approximate Bayesian computation approach [10] can be used to sample the intractable distribution, these algorithms are too computationally intensive for the Bayesian DOE because the problem requires sampling many different posteriors for each design candidate. A popular approach for alleviating the computational cost of the Bayesian DOE for nonlinear observational maps is using a Laplace approximation of the posterior distribution [11, 12, 13, 14]. In [15], Alexanderian et al. used the Laplace approximation of the posterior distribution in the context of the A-optimal DOE. In [16], Beck et al. used the Laplace approximation of the posterior density for estimating the expected information gain, which was later incorporated with the multilevel method in [17] and the stochastic gradient descent for finding the optimal design in [18]. Except for linear observation maps, the above mentioned approaches estimate the expected conditional quantities using three steps: first, sampling the posterior distribution or its approximation corresponding to each observational sample; second, estimating the posterior characteristic, *e.g.*, the posterior variance or the Kullback-Leibler divergences with respect to the prior; and finally, repeating the previous step for many observational samples to estimate the expected value of the posterior characteristics. The first two steps are equivalent to solving multiple different inverse problems, each of which is computationally expensive, in particular for high-dimensional cases, due to the *intractability* of the posterior distribution.

This paper presents a novel method for estimating the ECV using the projection-based approximation of the conditional expectation (PACE). The method is designed to handle computationally expensive observational maps parameterized by design parameters. The relationship between the uncertainty of the quantities of interest, represented by random variable (RV) Q , and their corresponding experimental observations, denoted as RV Y_d , is assumed to be $Y_d = h(Q, d) + \Xi$, where h is the observational map, Ξ represents measurement error, and d denotes the design parameters. The ECV of the RV Q given RV Y_d , denoted as $E[\text{Var}[Q | Y_d]]$, is obtained by approximating the conditional expectation (CE) using the law of total variance. Specifically, the ECV can be computed as the difference between the variance of Q and the variance of the CE $E[Q | Y_d]$. To approximate the CE, we utilize the orthogonality property of CE and introduce the map $\phi(Y_d)$, which minimizes the mean square error $E[\|Q - \phi(Y_d)\|_2^2]$ under the assumption of finite variances for Q and Y_d . The proposed approach avoids the need for sampling or approximating the posterior distribution and eliminates the evaluation of the likelihood function. Notably, we show that the relative mean absolute error of the PACE-based estimator of ECV is of the order $\mathcal{O}(N^{-2})$, where N represents the number evaluations of the observational map. Moreover, the computational efficiency of the proposed approach remains unaffected by the intractability of the posterior. In a related work by Hoang et al. [19], the application of the PACE approach in non-linear data assimilation problems was investigated. The findings from this study demonstrated that the conditional

mean filters outperform linear filters in terms of accuracy.

To implement our method, we select the artificial neural network (ANN) [20, 21] for approximating the CE, due to its versatility and demonstrated effectiveness in handling high-dimensional regression problems. For dealing with continuous design domains, we present a novel algorithm that effectively minimizes the ECV based on the stochastic gradient descent method. The algorithm employed for optimizing the design parameters is integrated with the training process of the ANN, resulting in improved computational efficiency. This integration is possible because the objective functions of optimizing the ECV and training the ANN are identical. Moreover, we propose a non-local approximation of the CE and apply transfer learning to reduce the number of evaluations of the observation model.

The rest of the paper is structured as follows. In Sec. 2, we summarize the background of Bayesian DOE. Sec. 3 details the PACE framework applied for the A-optimal DOE and its error estimation. In Sec. 4, we illustrate our method and verify the error estimation using the linear-Gaussian setting of the DOE. Then, in Sec. 5, we examine the scenario of the continuous design domain and develop a stochastic optimization algorithm for solving the A-optimal DOE. In Sec. 6, we apply our approach for the optimal design of electrical impedance tomography experiments used to identify composite material properties. Finally, in Sec. 7, the paper concludes with a summary and perspectives.

2 Background

In Bayesian DOE, we model the uncertainty associated with the quantities of interest to be identified as a RV, denoted here as Q and valued in \mathbb{R}^n . We consider a deterministic observational map, denoted as h , which is parameterized by design parameters d in a domain $\mathcal{D} \subset \mathbb{R}^\delta$. This map takes each vector $q \in \mathbb{R}^n$ and maps it to a noise-free observational vector in \mathbb{R}^m . We address the scenario where the model h consists of two components: a computationally expensive numerical model denoted as h_m , which solves the partial differential equation governing the experiments, and a measurement operator h_o . Typically, we have the relationship $h = h_o \circ h_m$. Assuming that the measurement error is additive, we model the observational RV Y_d for a given vector d of experimental design parameters as

$$Y_d(\omega) = h(Q(\omega), d) + \Xi(\omega), \quad (1)$$

where Ξ is the observational error RV, and ω denotes an outcome in the sample space Ω of the underlying probability space $(\Omega, \mathfrak{A}, \mathbb{P})$. Here, the subscript d indicates the dependence of the observational RV Y_d on the design parameters d . The inverse problem involves updating the knowledge of the quantities of interest given a specific vector of measurements y .

Bayesian identification framework is a standard approach for solving the inverse problem owing to its mathematically well-posedness and ability to account for uncertainty. Let us assume that the distributions of the RVs Q , Y_d , and Ξ are absolutely continuous, *i.e.*, their densities exist and have finite variances. For a fixed vector d , given the prior PDF π_Q of RV Q and the observational data y , the Bayesian posterior PDF $\pi_{Q|Y_d}(\cdot | y)$ is given as follows

$$\pi_{Q|Y_d}(q | y) = \frac{\pi_Q(q) \pi_\Xi(y - h(q, d))}{\pi_{Y_d}(y)}, \quad (2)$$

where $\pi_\Xi(y - h(q, d))$ is the likelihood function, and $\pi_{Y_d}(y)$ is the evidence given by

$$\pi_{Y_d}(y) = \int_{\mathbb{R}^n} \pi_Q(q) \pi_\Xi(y - h(q, d)) dq. \quad (3)$$

The method of Bayesian DOE seeks the parameters of experimental design that minimize the posterior uncertainty. Here, we consider the A-optimal DOE, which essentially minimizes the expected posterior variance. The posterior variance can be formulated via the Bayes' rule Eq. (2) as

$$\text{Var} [Q | y; d] = \int_{\mathbb{R}^n} q^{\odot 2} \pi_{Q|Y_d}(q|y) dq - \left[\int_{\mathbb{R}^n} q \pi_{Q|Y_d}(q|y) dq \right]^{\odot 2}, \quad (4)$$

where \odot is the Hadamard square operator, e.g., $q^{\odot 2} = [q_1^2, \dots, q_n^2]^\top$. To cover all possibilities of the measurement data, the A-optimal DOE examines the conditional variance $\text{Var} [Q | Y_d]$, which is an \mathbb{R}^n -valued RV defined as

$$\text{Var} [Q | Y_d] (\omega) \equiv \text{Var} [Q | Y_d(\omega); d]. \quad (5)$$

The A-optimal DOE approach seeks the experimental design's parameters that minimize the expected conditional variance of the RV Q given RV Y_d , denoted as $E[\text{Var} [Q | Y_d]]$. When dealing with multidimensional cases where $n > 1$, the A-optimal DOE approach uses the element-wise sum of the expected conditional variance as the objective function, referred to as the *total expected conditional variance* (tECV) in this paper. The tECV V for a given vector $d \in \mathbb{R}^\delta$ of experimental design parameters is given by

$$V(d) = \sum_{i=1}^n E[\text{Var} [Q_i | Y_d]] \quad (6)$$

where $\text{Var} [Q_i | Y_d]$ is the conditional variance i -th component of the RV Q . Another way to express the tECV is through the trace of the expected conditional covariance, which is given by $V(d) \equiv \text{tr}(\text{Cov} [Q | Y_d])$. Here, Cov is the covariance operator, and tr is the trace operator.

We obtain the A-optimal experimental design by minimizing the tECV, *i.e.*, its parameter vector $d_A \in \mathbb{R}^\delta$ satisfies:

$$d_A = \arg \min_d V(d). \quad (7)$$

By minimizing the tECV, the A-optimal DOE approach seeks to reduce the overall variability of the posterior.

Solving the optimization problem in Eq. (7) requires an efficient and accurate estimation of the tECV. Employing the MC method to estimate the tECV based on Eq. (6) requires a double-loop algorithm. The outer loop samples the RV Y_d while the inner loop estimates the posterior variance for each sample of the outer loop. Lets $\{y^{(i)}\}_{i=1}^{N_o}$ be N_o samples from the outer loop. Estimating the posterior variance $\text{Var} [Q | y^{(i)}; d]$ for each sample $y^{(i)}$ involves integrating with respect to (*w.r.t.*) the posterior distribution $\pi_{Q|Y_d}(\cdot | y^{(i)})$. However, both the sampling and approximating the posterior distribution pose a significant challenge due to the intractability of the posterior, *e.g.*, the posterior concentrates in significantly smaller regions compared to the prior, especially in high-dimensional problems where $n, m \gg 1$. Using the importance sampling (IS) method or the Markov-Chain Monte-Carlo (MCMC) method for computing the tECV becomes computationally expensive in such cases. The formulation of the IS double-loop estimator can be found in Appendix A. Enhancing the efficiency of the IS estimator is possible using the Laplace approximation. However, this method assumes that the underlying distribution closely resembles a Gaussian distribution and necessitates finding the maximum a posteriori estimator.

Notably, estimating the tECV involves applying the IS method to compute variances of N_o different posteriors, resulting in a multiplicative computational expense of order $N_o \times N_i$, where N_i is the number of samples in the inner loop. Similarly, other approaches that estimate tECV by sampling the posterior, such as the MCMC method, also suffer from the same multiplicative growth of computational expense. Here, we present a novel approach to approximate the tECV via the CE owing to the orthogonal projection of the CE. The approach does not require approximating or sampling the posterior distribution, as will be discussed in Sec. 3.

3 Estimation of the tECV using PACE

We demonstrate that the evaluation of the tECV ($V(d)$) can be accomplished via an approximation of the CE instead of sampling the conditional variance. For a given experimental parameter vector d , the CE of the RV Q given the RV Y_d , denoted as $E[Q | Y_d]$, satisfies

$$\int_A Q(\omega) d\mathbb{P}(\omega) = \int_A E[Q | Y_d](\omega) d\mathbb{P}(\omega), \quad (8)$$

for every measurable sets A in the σ -algebra generated by the RV Y_d . Following Doob–Dynkin lemma, the CE is a composition of a map $\phi_d : \mathbb{R}^m \rightarrow \mathbb{R}^n$ and the RV Y_d , given by

$$E[Q | Y_d](\omega) = \phi_d(Y_d(\omega)). \quad (9)$$

The map ϕ_d can be defined via the posterior density as

$$\phi_d(y) = \int_{\mathbb{R}^n} q \pi_{Q|Y_d}(q, y) dq. \quad (10)$$

Alternatively, the map ϕ_d can be obtained using the orthogonal projection property. For finite-variance RVs Q and Y_d , the CE $E[Q | Y_d]$ is the L_2 orthogonal projection of RV Q onto the σ -algebra generated by the RV Y_d , which is formulated as

$$E[Q | Y_d] = \phi_d(Y_d), \quad \text{where} \quad \phi_d = \arg \min_{f \in \mathcal{S}(\mathbb{R}^m, \mathbb{R}^n)} E \left[\|Q - f \circ Y_d\|_2^2 \right], \quad (11)$$

where $\|\cdot\|_2$ is the L_2 norm. Here, $\mathcal{S}(\mathbb{R}^m, \mathbb{R}^n)$ represents the set of all functions $f : \mathbb{R}^m \rightarrow \mathbb{R}^n$ for which the variance of the RV $f(Y_d)$ is finite. Appendix B.3 provides a proof of the orthogonal projection property. The general theoretical properties of the CE can be found in, *e.g.*, [22] and [23, Chapter 4]. The following proposition provides a formulation of the tECV expressed via the CE.

Proposition 1. *The total expected conditional variance $V(d)$ given in Eq. (6) can be expressed via CE $E[Q | Y_d]$ as:*

$$V(d) = E \left[\|Q - E[Q | Y_d]\|_2^2 \right]. \quad (12)$$

A proof of Proposition 1 is given in Appendix B.1. Based on Proposition 1, the tECV can be estimated by approximating the CE.

3.1 PACE-based MC estimator of the tECV

We leverage the orthogonal projection property described in Eq. (11) to approximate the CE, eliminating the necessity of sampling or approximating the posterior distributions as in Eq. (10). For nonlinear observational map h , the CE typically becomes nonlinear and does not admit a closed-form solution. In such cases, we employ the nonlinear regression method to approximate the CE, which involves three key components. First, we select a suitable parameterized functional subspace of finite dimension $\mathcal{S}'(\mathbb{R}^m, \mathbb{R}^n) \subset \mathcal{S}(\mathbb{R}^m, \mathbb{R}^n)$. This subspace represents a restricted set of functions used to approximate the CE. Second, solving the projection problem described in Eq. (11) within this chosen subspace. Last, we employ an appropriate MC estimator to estimate the MSE $E \left[\|Q - g \circ Y_d\|_2^2 \right]$.

By selecting \mathcal{S}' as the space of linear functions, we obtain a linear approximation of the CE, as detailed in Appendix C.1. However, this linear approximation of the CE is known to be biased

and tends to overestimate the tECV. The remainder of this section is dedicated to developing a suitable method for approximating the nonlinear CE.

Our primary objective in this section is to approximate the CE for a specific fixed vector of design parameters d . We will expand our approach in Sec. 5 to encompass the neighborhood surrounding a given vector d . Let $\boldsymbol{\theta} \in \mathbb{R}^\beta$ denote the vector of hyper-parameters of functions f in the selected sub-space \mathcal{S}' . We use the orthogonal projection property (Eq. (11)) to approximate the map ϕ_d by the function $f^* := f(\cdot; \boldsymbol{\theta}^*)$ in the subspace \mathcal{S}' such that

$$\boldsymbol{\theta}^* = \arg \min_{\boldsymbol{\theta}} \mathbb{E} \left[\|Q - f(Y_d; \boldsymbol{\theta})\|_2^2 \right]. \quad (13)$$

To simplify the notation, we introduce the MSE function $\mathcal{M} : \mathcal{S} \rightarrow \mathbb{R}_+$ defined as

$$\mathcal{M}(f) \equiv \mathbb{E} \left[\|Q - f(Y_d)\|_2^2 \right]. \quad (14)$$

With this notation in place, the relation among functions in \mathcal{S} can be summarized as:

$$\mathcal{M}(f) \geq \mathcal{M}(f^*) \geq \mathcal{M}(\phi_d) = V_d, \quad \forall f \in \mathcal{S}'.$$

A straightforward method to estimate the MSE $\mathcal{M}(f)$ is using the crude Monte Carlo (MC) method. Let $D_N = \{(q^{(i)}, y^{(i)})\}_{i=1}^N$ be an N -sized dataset of *i.i.d.* samples of the pair RVs (Q, Y_d) , where $\{q^{(i)}\}_{i=1}^N$ are *i.i.d.* samples of RV Q , and $\{y^{(i)}\}_{i=1}^N$ are the corresponding *i.i.d.* samples of RV Y_d obtained as

$$\{y^{(i)}\}_{i=1}^N = \left\{ y^{(i)} \mid y^{(i)} = h(q^{(i)}, d) + \xi^{(i)}, \quad q^{(i)} \in \{q^{(i)}\}_{i=1}^N \right\}. \quad (15)$$

Here, $\{\xi^{(i)}\}_{i=1}^N$ are *i.i.d.* samples of Ξ .

Let $D_M = \{(q^{(i)}, y^{(i)})\}_{i=1}^M$ be an M -sized dataset of *i.i.d.* samples of the pair RVs (Q, Y_d) statistically independent from D_N . We denote the crude MC estimator of the MSE $\mathcal{M}(f)$ using a dataset $D \in \{D_N, D_M\}$ as:

$$\widehat{\mathcal{M}}(f \mid D) = \frac{1}{|D|} \sum_{(q,y) \in D} \|q - f(y)\|_2^2, \quad (16)$$

where $|D|$ is the cardinality of the dataset D . Owing to Proposition 1, we estimate the tECV using the following *PACE-based MC estimator* $\widehat{V}_d(D_N, D_M)$:

$$\widehat{V}_d(D_N, D_M) := \widehat{\mathcal{M}}(f(\cdot; \boldsymbol{\theta}_{D_N}) \mid D_M) \quad (17a)$$

$$\text{where } \boldsymbol{\theta}_{D_N} = \arg \min_{\boldsymbol{\theta}} \widehat{\mathcal{M}}(f(\cdot; \boldsymbol{\theta}) \mid D_N), \quad (17b)$$

which requires numerically solving the optimization problem stated in Eq. (17b). We observe that unlike the double-loop estimator using IS, which incurs a computational cost proportional to the product $(N_o \times N_i)$ as explained in Sec. 2, the PACE-based approach exhibits a linear cost proportional to the sizes of datasets D_N and D_M .

Although the PACE-based approach requires solving a regression problem for approximating the CE, it completely avoids the need for sampling or approximating different posterior densities. This allows us to bypass the complication associated with posterior intractability. Using the regressor, we obtain approximate values of the CE's samples with minimal computing effort. In the remaining part of this section, we analyze the statistical error of the PACE-based MC estimator $\widehat{V}_d(D_N, D_M)$ and propose a control-variate estimator to replace the crude MC one, $\widehat{\mathcal{M}}(f \mid D)$.

3.2 Estimation of errors

Here, we aim to analyze the mean absolute error of the estimator (MAE) $\widehat{V}_d(D_N, D_M)$ compared with the target one V_d . Let $\epsilon_{S'}$, ϵ_{opt} , and ϵ_{MC} denote the approximation error due to the choice of the sub-space S' , the optimization error in numerically solving the minimization problem stated in Eq. (17b) with the finite-size dataset D_M , and the estimating error of the MC estimator due to the finite-size of the dataset D_N , respectively, *i.e.*,

$$\epsilon_{S'} := \mathbb{E} [|\mathcal{M}(f^*) - \mathcal{M}(\phi_d)|], \quad (18)$$

$$\epsilon_{\text{opt}} := \mathbb{E} [|\mathcal{M}(f(\cdot; \boldsymbol{\theta}_{D_N})) - \mathcal{M}(f^*)|], \quad (19)$$

$$\epsilon_{\text{MC}} := \mathbb{E} \left[\left| \widehat{\mathcal{M}}(f(\cdot; \boldsymbol{\theta}_{D_N}) \mid D_M) - \mathcal{M}(f(\cdot; \boldsymbol{\theta}_{D_N})) \right| \right]. \quad (20)$$

The MAE between the estimator $\widehat{V}_d(D_N, D_M)$ and V_d is bounded using the triangular inequality as:

$$\begin{aligned} \mathbb{E} \left[\left| \widehat{V}_d(D_N, D_M) - V_d \right| \right] &= \mathbb{E} \left[\left| \widehat{\mathcal{M}}(f(\cdot; \boldsymbol{\theta}_{D_N}) \mid D_M) - \mathcal{M}(\phi_d) \right| \right] \\ &\leq \mathbb{E} \left[\left| \widehat{\mathcal{M}}(f(\cdot; \boldsymbol{\theta}_{D_N}) \mid D_M) - \mathcal{M}(f(\cdot; \boldsymbol{\theta}_{D_N})) \right| \right] \\ &\quad + \mathbb{E} [|\mathcal{M}(f(\cdot; \boldsymbol{\theta}_{D_N})) - \mathcal{M}(f^*)|] \\ &\quad + \mathbb{E} [|\mathcal{M}(f^*) - \mathcal{M}(\phi)|] \\ &= \epsilon_{\text{MC}} + \epsilon_{\text{opt}} + \epsilon_{S'}. \end{aligned} \quad (21)$$

Aiming at an asymptotic error estimator that captures the evolution of the error *w.r.t.* the sizes of datasets D_N and D_M , we make use of the following assumptions:

Assumption 1. S' is a convex set and contains constant functions.

Assumption 2.

$$\text{Var} \left[\|Q - f^*(Y_d)\|_2^2 \right] = \mathcal{O} \left(2 \mathbb{E} \left[\|Q - f^*(Y_d)\|_2^2 \right]^2 \right) < \infty. \quad (22)$$

Assumption 3.

$$\epsilon_{\text{opt}} = \mathcal{O} \left(\mathbb{E} \left[\left| \widehat{\mathcal{M}}(f^* \mid D_N) - \mathcal{M}(f^*) \right| \right] \right). \quad (23)$$

The first assumption is a common constraint on choosing the subspace S' . This assumption implies that $\mathbb{E} \left[(Q - f^*(Y_d))^\top g(Y_d) \right] = 0$ for every $g \in S'$. By choosing g as constant functions, we obtain that the mean of the RV $Q - f^*(Y_d)$ is zero. The second assumption is motivated by the fact that for every zero-mean Gaussian RV X , we have $\text{Var} [X^2] = \mathbb{E} [X^4] - (\mathbb{E} [X^2])^2 = 2(\mathbb{E} [X^2])^2$. The third assumption suggests that the error of the optimization problem under the finite-sized dataset D_N is in the same order as the statistical error of the MC estimator $\widehat{\mathcal{M}}(f^* \mid D_N)$.

Proposition 2 (Error estimation). *Assuming that RVs Q and Y_d have finite variances, and that the Assumptions 1, 2, and 3 hold, the MAE of the PACE-based MC estimator $\widehat{V}_d(D_N, D_M)$ satisfies:*

$$\mathbb{E} \left[\left| \widehat{V}_d(D_N, D_M) - V_d \right| \right] = \mathcal{O} \left(\left(\frac{2}{\sqrt{\pi N}} + \frac{2}{\sqrt{\pi M}} \right) \mathbb{E} \left[\|Q - f^*(Y_d)\|_2^2 \right] \right) + \epsilon_{S'}. \quad (24)$$

as $N, M \rightarrow \infty$.

If we further assume that the approximation error $\epsilon_{S'} = 0$, then

$$\begin{aligned} \mathbb{E} \left[|\widehat{V}_d(D_N, D_M) - V_d| \right] &= \mathcal{O} \left(\left(\frac{2}{\sqrt{\pi N}} + \frac{2}{\sqrt{\pi M}} \right) \mathbb{E} \left[\|Q - f^*(Y_d)\|_2^2 \right] \right) \\ &= \mathcal{O} \left(\left(\frac{2}{\sqrt{\pi N}} + \frac{2}{\sqrt{\pi M}} \right) \mathbb{E} \left[\|Q - \phi_d(Y)\|_2^2 \right] \right) \\ &= \mathcal{O} \left(\frac{2}{\sqrt{\pi N}} + \frac{2}{\sqrt{\pi M}} \right) V_d \end{aligned} \quad (25)$$

Let relMAE (\widetilde{V}_d) be the relative MAE of an estimator \widetilde{V}_d of V_d , defined as:

$$\text{relMAE}(\widetilde{V}_d) \equiv \frac{\mathbb{E} \left[|\widetilde{V}_d - V_d| \right]}{V_d}. \quad (26)$$

When $\epsilon_{S'} = 0$, the relative MAE of the estimator $\widehat{V}_d(D_N, D_M)$ is given by

$$\begin{aligned} \text{relMAE}(\widehat{V}_d) &\equiv \frac{\mathbb{E} \left[|\widehat{V}_d(D_N, D_M) - V_d| \right]}{V_d} \\ &= \mathcal{O} \left(\frac{2}{\sqrt{\pi N}} + \frac{2}{\sqrt{\pi M}} \right). \end{aligned} \quad (27)$$

When upper bounds of the errors $\epsilon_{S'}$, ϵ_{opt} , and ϵ_{MC} are available, it is feasible to derive a more precise bound for the MAE of the PACE-based MC estimator. However, such bounds are problem-dependent and beyond the scope of this paper.

3.3 Reduced variance estimator

We often model the measurement error RV Ξ using simple parameterized distributions such as Gaussian distribution, Poisson distribution, or binomial distribution. Consequently, sampling the RV Ξ is computationally cheap. Based on this observation, we augment the datasets D_N and D_M to reduce the statistical error of the PACE-based MC estimators. The augmented datasets can be obtained as:

$$D_N^{\text{rv}} = \left\{ \left(q^{(i)}, y^{(i,j)} \right) \mid y^{(i,j)} = h(q^{(i)}, d) + \xi^{(i,j)} \right\}_{i=1, \dots, N, j=1, \dots, a}, \quad (28)$$

$$D_M^{\text{rv}} = \left\{ \left(q^{(i)}, y^{(i,j)} \right) \mid y^{(i,j)} = h(q^{(i)}, d) + \xi^{(i,j)} \right\}_{i=1, \dots, M, j=1, \dots, a}, \quad (29)$$

where $q^{(i)}$ and $\xi^{(i,j)}$ are *i.i.d.* samples of RVs Q and Ξ , and $a \in \mathbb{N}_+$ represents the augmentation multiplier. By substituting the augmented datasets D_N^{rv} and D_M^{rv} for D_N and D_M respectively, in Eq. (16) we obtain the reduced variance estimators of the MSE $\widehat{\mathcal{M}}(f \mid D_N)$ and $\widehat{\mathcal{M}}(f \mid D_M)$ as follows:

$$\begin{aligned} \widehat{\mathcal{M}}^{\text{rv}}(f \mid D_N) &= \frac{1}{|D_N| \times a} \sum_{(q,y) \in D_N^{\text{rv}}} \|q - f(y)\|_2^2 \\ \widehat{\mathcal{M}}^{\text{rv}}(f \mid D_M) &= \frac{1}{|D_M| \times a} \sum_{(q,y) \in D_M^{\text{rv}}} \|q - f(y)\|_2^2. \end{aligned} \quad (30)$$

Appendix D explains the reduction of the statistical error gained by using the estimator $\widehat{\mathcal{M}}^{\text{rv}}$ compared to the crude one.

4 Numerical experiment: linear-gaussian setting

In this section, we present the results of numerical experiments to demonstrate the error estimation outlined in Sec. 3.2. We focus on the linear-Gaussian scenario, where both distributions of the prior and the measurement error are Gaussian, and the observational map is linear. This setting is advantageous for error analysis because it allows for an analytical solution for the tECV. We will expand our numerical experiments to a broader nonlinear setting in Sec. 6.

To assess the effectiveness of the PACE-based approach, we conduct numerical experiments in two different scenarios. In Sec. 4.1, we apply our method to a one-dimensional setting where $d \in \mathbb{R}$, while in Sec. 4.2, we evaluate our approach in a high-dimensional scenario. Furthermore, we compare the performance of the PACE-based approach with that of the IS-based approach, focusing on examining the effect of two factors: (1) increasing the dimension of the inferred parameters vector q , and (2) reducing the measurement errors. These factors significantly exacerbate the intractability issues associated with the IS-based approach outlined in Appendix A.

4.1 One-dimensional case

In this section, we consider the following setting:

$$h(Q, d) = \frac{Q}{(d - 0.5)^2 + 1}, \quad d \in [0, 1], \quad (31a)$$

$$Q \sim \mathcal{N}(0, \sigma_q^2), \quad \text{with } \sigma_q = 2, \quad (31b)$$

$$\Xi \sim \mathcal{N}(0, \sigma_\xi^2), \quad (31c)$$

where $\mathcal{N}(0, \sigma^2)$ is a Gaussian distribution of zero-mean and variance σ^2 . We analyze two cases of measurement error variance: $\sigma_\xi^2 = 0.01^2$ and $\sigma_\xi^2 = 0.001^2$. Given that the observational map is linear in terms of q , and both the prior and measurement error distributions are Gaussian, the CE's map ϕ_d defined in Eq. (11) is linear and possesses a closed-form expression. Indeed, we have

$$\phi_d(y) = \frac{a\sigma_q^2}{a^2\sigma_q^2 + \sigma_\xi^2} y, \quad \text{where } a = \frac{1}{(d - 0.5)^2 + 1}. \quad (32)$$

Appendix C.1 provides a detailed explanation of this linear approximation.

To implement our method in this setting, we employ linear regression to empirically approximate the CE by solving Eq. (11) within the sub-space S' of linear functions given the samples dataset $D_N = \{(q^{(i)}, y^{(i)})\}_{i=1}^N$. For detailed information, please refer to Appendix C.2. We then utilize the obtained CE approximation to estimate the tECV using Eq (30). To assess the accuracy of our estimation, we compute the empirical relative MAE metric defined in Eq.(26). In particular, we aim to compare the empirical relative MAE with our estimation in Eq.(27), considering the absence of bias error $\epsilon_{S'}$ in this linear-Gaussian setting. Additionally, we implement the IS-based approach described in Appendix A to estimate the tECV and evaluate its relative MAE.

Based on the result of Proposition 2, setting $N \equiv M$ is a straightforward choice for the PACE-based approach. In the IS-based approach, the ECV is estimated using a double-loop MC algorithm, as detailed in Appendix A. Because the posterior variance remains invariant *w.r.t* y in this linear-Gaussian setting, we set the number of samples for the outer loop as $N_o = 1$. In the PACE-based approach, the total number of samples is $N + M$, while for the IS-based approach, it is $N_i + 1$, with N_i representing the number of samples for the inner loop. Fig. 1 shows the relative MAE for $d = 0.5$ for two different measurement variances, $\sigma_\xi^2 = 0.01^2$ and $\sigma_\xi^2 = 0.001^2$. Fig. 2 showcases the tECV for different values of d and $\sigma_\xi^2 = 0.01^2$. To estimate the relative MAE, we perform 1000 statistically independent simulations.

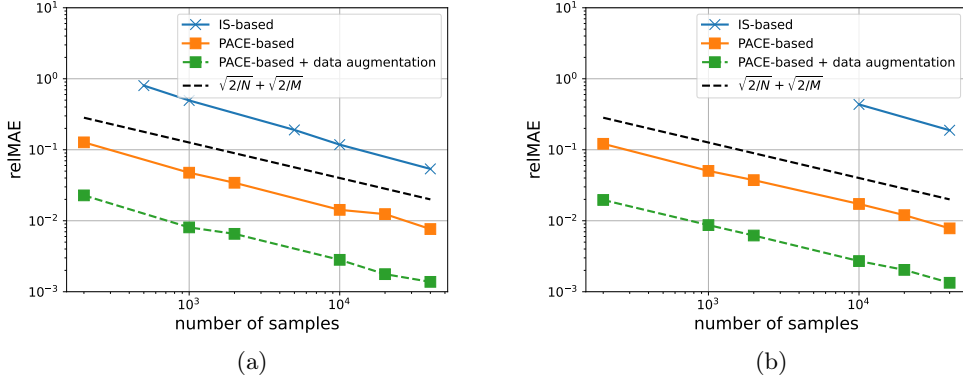


Figure 1: Comparison of the PACE and IS-based approaches for estimating the tECV for $d = 0.5$: (a) $\Xi \sim \mathcal{N}(0, 0.01^2)$ and (b) $\Xi \sim \mathcal{N}(0, 0.001^2)$.

As observed from Fig. 1, the PACE-based method without data augmentation achieves a similar relative MAE metric with significantly fewer samples compared with the IS-based approach. For example, for $\sigma_\xi^2 = 0.01^2$, the required number of samples is reduced by approximately 30 times, and for $\sigma_\xi^2 = 0.001^2$, it is reduced by 200 times. When using data augmentation, our approach further reduces the number of samples by nearly two more orders of magnitude.

Overall, the empirical relative MAE confirms the theoretical one, *i.e.*, $\mathcal{O}\left(\frac{2}{\sqrt{\pi N}} + \frac{2}{\sqrt{\pi M}}\right)$, as obtained in Proposition 2. Particularly, we have $\text{Var}\left[(Q - f^*(Y_d))^2\right] = 2\text{E}\left[(Q - f^*(Y_d))^2\right]^2$, which validates Assumption 2. Since the CE in this example is a linear function, ϵ_{opt} is much smaller than the estimated order $\left(\text{E}\left[\left|\widehat{\mathcal{M}}(f^*|D_N) - \mathcal{M}(f^*)\right|\right]\right)$ assumed in the Assumption 3. Consequently, the obtained relative MAE is consistently smaller than its theoretical estimated order $\left(\frac{2}{\sqrt{\pi N}} + \frac{2}{\sqrt{\pi M}}\right)$.

We also observe that our method exhibits invariant of the relative MAE *w.r.t.* the measurement error variance. In contrast, the IS-based method requires significantly larger numbers of samples. In particular, diminishing the measurement error variance reduces the denominator in Bayes' rule. Consequently, the statistical error inherent in the IS-based approach is amplified.

Fig. 2 clearly illustrates that the PACE-based approach accurately estimates the optimal design, *i.e.*, $d_A = 0.5$, with 10000 samples. However, the IS-based approach results in significant errors in identifying the optimal design due to its statistical errors in estimating the tECV.

4.2 High-dimensional case

In this section, we address the high-dimensional linear-Gaussian scenario. The setting is described as follows:

$$\begin{aligned}
 G(q, d) &= \frac{1}{(d - 0.5)^2 + 1} Q, \quad d \in [0, 1], \\
 Q &\sim \mathcal{N}(0_n, \mathbf{I}_n), \\
 \Xi &\sim \mathcal{N}(0_n, 0.1^2 \mathbf{I}_n),
 \end{aligned} \tag{33}$$

where $0_n \in \mathbb{R}^n$ and $\mathbf{I}_n \in \mathbb{R}^{n \times n}$ represent a zero vector and an identity matrix, respectively. We perform a similar analysis as presented in Sec. 4.1.

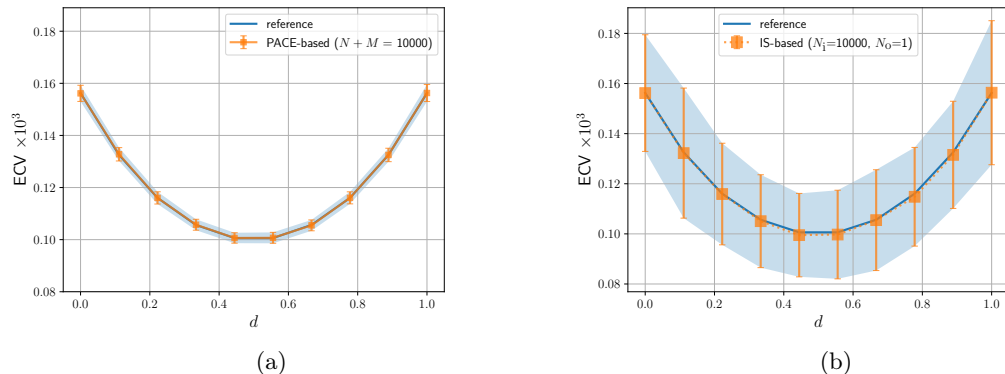


Figure 2: Comparison of the PACE and IS-based approaches for estimating the ECV with $\Xi \sim \mathcal{N}(0, 0.01^2)$ using 10000 samples: (a) PACE-based approach and (b) IS-based approach. The error bar plot depicts the empirical mean and standard deviation of the estimated values obtained by running 1000 statistically independent MC simulations.

Fig. 3 illustrates the relative MAE for different values of $n \in \{2, 5, 10, 20\}$. The numerical results demonstrate that the IS-based approach requires a significantly large number of samples for high-dimensional cases. Specifically, for $n \geq 5$, we do not observe the convergence of the IS-based approach. For $n = 20$, the IS-based approach frequently returns a not-a-number error due to the diminishing evidence term in the Bayes' rule, see Eq. (3). In contrast, our PACE-based approach effectively mitigates the curse of dimensionality.

5 Stochastic optimization for the continuous design domain

The PACE approach can be straightforwardly applied to solve the A-ODE problem on a discrete and finite design domain. Using the PACE approach, one can estimate the tECV for each experimental design, and the design with the minimum tECV is considered the optimal solution. In this section, we shift our focus to the continuous design domain. We assume that the gradient of the measurement map *w.r.t.* design parameters, $\nabla_d h$, exists and can be numerically computed. To solve the A-ODE problem efficiently, we incorporate stochastic gradient descent techniques with the PACE-based reduced variance MC estimator of tCEV.

When utilizing stochastic gradient optimization algorithms to solve the A-DOE problem, the computation of the gradient of the tCEV *w.r.t.* the design parameters, denoted as $\nabla_d V_d$, can pose a challenge. To address this issue, we propose a non-local approximation of the CE. Our approach involves approximating the CE within a neighborhood surrounding a given design parameter vector, enabling the evaluation of $\nabla_d V_d$. We utilize artificial neural networks (ANNs) as the approximation tool, although other regression techniques can also be incorporated into our method.

Let $f_N(\cdot; \boldsymbol{\theta}) : \mathbb{R}^{m+\delta} \rightarrow \mathbb{R}^n$ be an ANN map, where $\boldsymbol{\theta}$ denotes its hyper-parameters. The proposed ANN takes inputs from a concatenation of a m -dimensional vector y and a δ -dimensional vector d . By combining Eqs. (7), (11), and (12) the A-optimal design parameter vector d_A is obtained by solving the following optimization problem

$$d_A = \arg_d \min_{d, \boldsymbol{\theta}} \mathbb{E} \left[\|Q - f_N(Y_d, d; \boldsymbol{\theta})\|_2^2 \right] \quad (34)$$

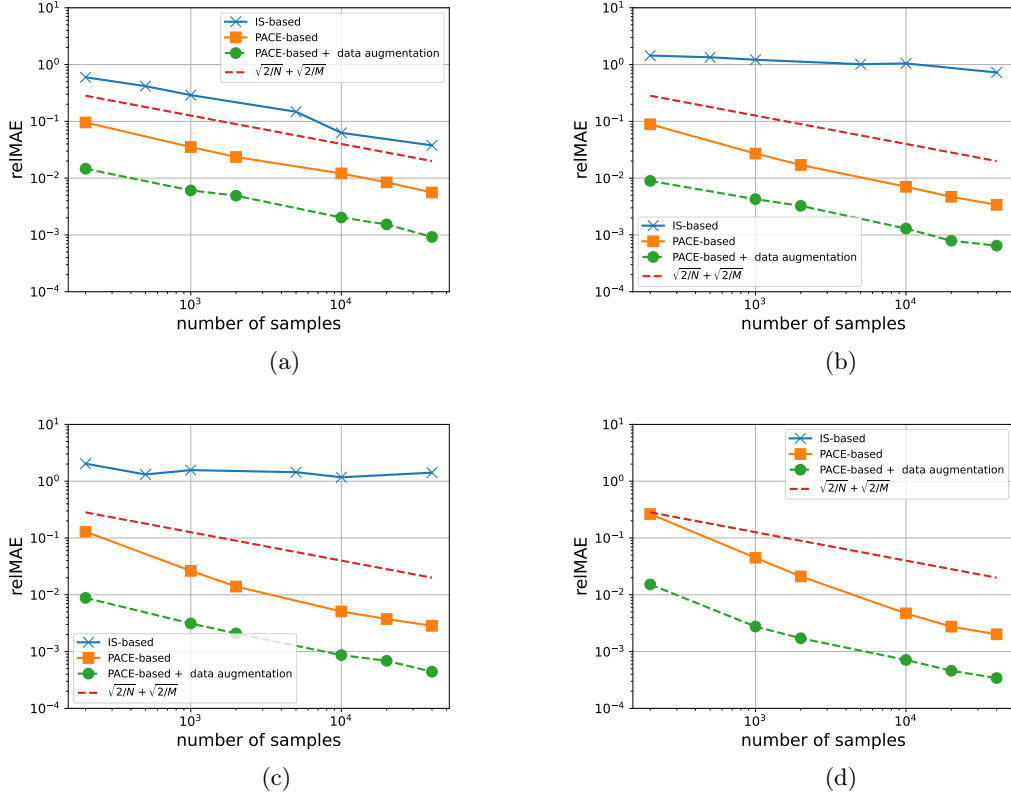


Figure 3: Comparison of the PACE and IS-based approach for high-dimensional linear examples: (a) $n = 2$, (b) $n = 5$, (c) $n = 10$, and (d) $n = 20$. For $n = 20$, all 100 statistically independent MC simulations using the IS-based approach return a *not-a-number* error. Consequently, its numerical results are not available.

which minimizes the MSE *w.r.t.* both the ANN’s hyper-parameters and the design parameters. In other words, the optimization problems for approximating the CE and seeking the A-optimal design minimize an identical objective function.

In the course of an iterative optimization process to solve Eq. (34), when the algorithm provides a new candidate vector for d_A , the ANN may need to be retrained. Here, we employ the transfer learning technique, *i.e.*, the weights trained for the previous design candidate are used as the starting point for the current training process. This simple transfer learning technique efficiently reduces the training time and data required. In the rest of this section, we provide a more detailed explanation of the non-local approximation of the CE in Sec. 5.1 and discuss the algorithms used for implementing our method in Sec. 5.2.

5.1 Non-local approximation of the conditional expectation

Given a design candidate d_κ , we select a PDF w_κ defined over the design domain \mathcal{D} such that $w_\kappa(d) := \frac{w(d, d_\kappa)}{c}$. Here $w(d, d_\kappa)$ is a weight function such as a kernel, and c is a normalization constant defined as $c := \int_{\mathcal{D}} w(d, d_\kappa) dd < \infty$. In our notation, $\kappa \in \mathbb{N}_+$ denotes the iteration counter of the main procedure, which will be discussed in Sec. 5.2.

To approximate the CE in the neighborhood of a design d_κ , we determine the hyperparameters $\boldsymbol{\theta}_\kappa$ of the ANN f_N by solving the optimization problem:

$$\boldsymbol{\theta}_\kappa = \arg \min_{\boldsymbol{\theta}} L_\kappa(\boldsymbol{\theta}), \quad (35)$$

where L_κ is the weighted MSE function defined as

$$L_\kappa(\boldsymbol{\theta}) = \int_{\mathcal{D}} \mathbb{E} \left[\|Q - f_N(Y_d, d; \boldsymbol{\theta})\|_2^2 \right] w_\kappa(d) dd. \quad (36)$$

We use the variance reduction technique, similarly to Eq. (30), to approximate the function L_κ as

$$\widehat{L}_\kappa^{\text{vr}}(\boldsymbol{\theta}) = \frac{1}{N \times a} \sum_{i=1}^N \sum_{j=1}^a \left\| q^{(i)} - f_N(y^{(i,j)}, d^{(i)}; \boldsymbol{\theta}) \right\|_2^2, \quad (37)$$

where $q^{(i)}$ are *i.i.d.* samples of RV Q , $d^{(i)}$ are *i.i.d.* samples generated following the PDF w_κ , and $y^{(i,j)} = h(q^{(i)}, d^{(i)}) + \xi^{(i,j)}$ with $\xi^{(i,j)}$ being *i.i.d.* samples of RV Ξ .

A simple choice for the kernel function is the density of a multivariate Gaussian distribution, where the marginal variances serve as tuning parameters. Intuitively, increasing the marginal variances of the PDF w_κ reduces the error of the CE approximation over the entire design domain. However, it also requires a considerably larger number of samples for accurately estimating the weighted MSE $\widehat{L}_\kappa^{\text{vr}}$. In our algorithm, discussed in more detail in Sec. 5.2, for the κ -th iteration, we need only to evaluate the tECV and its derivative in the neighborhood of d_κ . Therefore, the tuned variances of the PDF η_κ are much smaller than the characteristic size of the design domain, which improves the computational efficiency by reducing the number of samples required to estimate the weighted MSE $\widehat{L}_\kappa^{\text{vr}}$.

5.2 Algorithm

We present a stochastic gradient descent algorithm in this section to solve Eq. (34). The algorithm utilizes the non-local approximation of the CE to estimate the tECV V_d and its derivative $\nabla_d V_d$. A typical κ -th iteration of the proposed algorithm consists of two steps:

- i) Given a design parameter candidate $d_{\kappa-1}$, we update the hyper-parameters $\boldsymbol{\theta}_\kappa$ by solving Eq. (35), for which *transfer learning* is applied,
- ii) We update the design parameter candidate based on the gradient field of the MSE *w.r.t* d , *i.e.*, $\nabla_d \mathbb{E} [\|Q - f_N(Y_d, d; \boldsymbol{\theta}_\kappa)\|_2^2]$. This step returns an updated candidate d_κ .

Algorithm 1 summarizes the main procedure, which calls the sub-optimization procedures corresponding steps i) and ii) described in Algorithms 2 and 3, respectively. The sub-optimization procedures in each step can be executed using the Adam algorithm [24].

Algorithm 1 Main

Require: Observational model, its derivatives ($\nabla_d h$), and number of iteration K

- 1: Initiate a value for d_0
 - 2: **for** κ from 1 to K **do**
 - 3: approximating the conditional expectation using Algorithm 2 $\rightarrow \boldsymbol{\theta}_\kappa$
 - 4: solving $\arg \min_d \mathbb{E} [\|Q - f_N(Y_d, d; \boldsymbol{\theta}_\kappa)\|_2^2]$ using Algorithm 3 $\rightarrow d_\kappa$
 - 5: **end for**
 - 6: **return** $d_A \leftarrow d_K$
-

In Algorithm 2, we generate *i.i.d.* samples $\{d^{(i)}\}_{i=1}^N$, $\{q^{(i)}\}_{i=1}^N$, and $\{\xi^{(i)}\}_{i=1}^N$ following PDFs w_κ , π_Q , and π_Ξ , respectively. Next, we use those samples to compute the samples of the observational RV, $y^{(i,j)} = h(q^{(i)}, d^{(i)}) + \xi^{(i,j)}$ for $j = 1, \dots, a$. Finally, we employ an Adam optimizer to train the ANN. We use the dataset $\{(q^{(i)}, d^{(i)}, y^{(i,j)})\}_{i=1, \dots, N; j=1, \dots, a}$ and the loss function $\widehat{L}_\kappa^{\text{vr}}$ (defined in Eq. (37)) for this training.

To reduce the numbers of epochs (e_1) and data samples ($N \times a$), we employ the *transfer learning* technique [25, 26], which re-uses the hyper-parameters obtained from the previous iteration, $\theta_{\kappa-1}$, as the initial value for the current iteration κ .

Algorithm 2 Non-local approximation of the CE operator

Require: d_κ , weight function $w(\cdot; d_\kappa)$, number of epoch e_1 , and learning rate α_1

- 1: Generate $\{d^{(i)}\}_{i=1}^N \sim w_\kappa(d)$, $\{q^{(i)}\}_{i=1}^N \sim \pi_Q$, $\{\xi^{(i,j)}\}_{i=1, \dots, N; j=1, \dots, a} \sim \pi_\Xi$
 - 2: Evaluate $\{h(q^{(i)}, d^{(i)})\}_{i=1}^N$
 - 3: Compute samples $\{y^{(i,j)}\}_{i=1, \dots, N; j=1, \dots, a}$ where $y^{(i,j)} = h(q^{(i)}, d^{(i)}) + \xi^{(i,j)}$
 - 4: Collect data into a dataset $D_N^{\text{vr}} = \{(q^{(i)}, d^{(i)}, y^{(i,j)})\}_{i=1, \dots, N; j=1, \dots, a}$
 - 5: Train the ANN using the initial weights $\theta_{\kappa-1}$ with e_1 epoch, Adam algorithm, learning rate α_1 , loss function $\widehat{L}_\kappa^{\text{vr}}$ defined in Eq. (37) and dataset D_N^{vr}
 - 6: **return** Hyper-parameters θ_κ of ANN f_N
-

In Algorithm 3, we generate *i.i.d.* samples $\{q^{(i)}\}_{i=1}^M$ following PDF π_Q . The dataset $\{q^{(i)}\}_{i=1}^M$ is divided into different batches of size M_b , denoted as $\{B_1, \dots, B_\beta\}$. For each batch B and a design candidate d_0 , we compute the corresponding samples of the observational RV as $y^{(i,j)} = h(q^{(i)}, d_0) + \xi^{(i,j)}$, where $q^{(i)} \in B$, $j = 1, \dots, a$, and $\xi^{(i,j)}$ are *i.i.d.* samples of the RV Ξ . We then update the design parameter as

$$d' = d_0 - \frac{\alpha_2}{M_b \times a} \sum_{i=1}^{M_b} \sum_{j=1}^a \nabla_d \left[\|q - f_N(h(q, d) + \xi, d)\|_2^2 \right] (q^{(i)}, y^{(i,j)}, d_0) \quad (38)$$

where α_2 is a learning rate. Here, $\nabla_d \left[\|q - f_N(h(q, d) + \xi, d)\|_2^2 \right] (q^{(i)}, y^{(i,j)}, d_0)$ represents the gradient of $\|q - f_N(h(q, d) + \xi, d)\|_2^2$ *w.r.t.* d , evaluated at $(q^{(i)}, y^{(i,j)}, d_0)$. The value of d' is then assigned to d_0 for the next batch.

Algorithm 3 Minimizing the MSE $E[\|Q - f_N(Y_d, d; \theta_\kappa)\|_2^2]$ *w.r.t.* d

Require: Observational model (h) and its derivatives ($\nabla_d h$), map $f_N(\cdot; \theta_\kappa)$ from Algorithm 2, d_κ , number of samples M , number of epoch e_2 , batch-size M_b , and learning rate α_2

- 1: $d_0 \leftarrow d_\kappa$
 - 2: Generate samples $\{q^{(i)}\}_{i=1}^M$ following prior PDF π_Q
 - 3: **for** $e = 1$ to e_2 **do**
 - 4: **for** $b = 1$ to M/M_b **do**
 - 5: Generate samples $\{\xi^{(i,j)}\}_{i=1, \dots, M_b; j=1, \dots, a}$ of the measurement error Ξ
 - 6: Evaluate $y^{(i,j)} = h(q^{(i)}, d_0) + \xi^{(i,j)}$
 - 7: Updating the design candidate using Adam algorithm based on Eq. (38).
 - 8: $d_0 \leftarrow d'$
 - 9: **end for**
 - 10: **end for**
 - 11: **return** $d_{\kappa+1} \leftarrow d_0$
-

In Appendix E, we use chain rule to derive the formulation of the gradient $\nabla_d \left[\|q - f_N(h(q) + \xi, d)\|_2^2 \right] (q^{(i)}, y^{(i,j)}, d_0)$ in terms of the gradients of the observational map h and the ANN f_N *w.r.t* d . Notably, for the ANN function f_N , its gradient is obtained straightforwardly using the back-propagation [27].

6 Numerical experiment: Electrical impedance tomography

Electrical impedance tomography (EIT) aims to determine the conductivity of a closed body by measuring the potential of electrodes placed on the body surface in response to applied electric current. In this section, we revisit an experimental design problem that was previously studied in [16, 17, 18]. The objective of the experiment is to recover the fiber orientation in each orthotropic ply of a composite laminate material based on potential measurements resulted from injecting low-frequency electric currents through electrodes attached to the body surface. The formulation of the EIT experiment is described in Sec. 6.1, where we adopt the complete electrode model from [28].

Previous studies employed the maximization of expected information gain (EIG) as the optimal criterion and estimated the EIG using the IS technique combined with the Laplace approximation of the posteriors. In Sec. 6.2, we begin by analyzing our PACE-based approach for estimating the tECV and comparing it with the IS-based technique. Subsequently, we utilize the optimization algorithms discussed in Sec. 5 to solve the DOE problem and present the numerical results.

6.1 Formulation and finite element model of EIT experiment

The rectangular body \mathcal{B} with boundary ∂B consists of two plies $\mathcal{B} = \bigcup_{i=1}^2 \mathcal{B}_i$. The surfaces of the exterior boundary are equipped with N_{el} electrodes on the area $E_1, \dots, E_{N_{\text{el}}}$.

These electrodes are used to apply known currents, and they also allow us to measure the electric potential. The configuration used in this work is illustrated in Fig. 4.

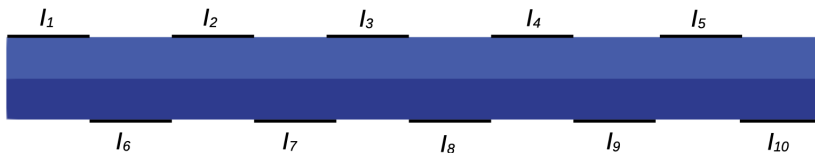


Figure 4: Sketch of the EIT experiment for a two-ply composite sample. The back rectangles indicate the electrode positions, and I_1, \dots, I_{10} are their applied currents.

The fiber orientation over the body \mathcal{B} is modeled as a random field $\eta : \mathcal{B} \times \Omega \rightarrow [-\pi, \pi]$ as follows:

$$\eta(x, \omega) = \begin{cases} \eta_1(\omega) & \text{in } \mathcal{B}_1, \\ \eta_2(\omega) & \text{in } \mathcal{B}_2. \end{cases} \quad (39)$$

The RV Q in this example is random vector valued in $[-\pi, \pi]^2$ representing the prior distribution of the fiber orientations of the plies, defined as

$$Q(\omega) := [\eta_1(\omega), \eta_2(\omega)]^\top. \quad (40)$$

We represent the quasi-static current flux and the quasi-static potential as random fields as $\zeta : \mathcal{B} \times \Omega \rightarrow \mathbb{R}^3$ and $u : \mathcal{B} \times \Omega \rightarrow \mathbb{R}$, respectively. The electrical current field and the potential

field satisfies the following PDE:

$$\begin{aligned}\nabla \cdot \zeta &= 0, \\ \zeta &= \sigma(\eta) \nabla u,\end{aligned}\tag{41}$$

where σ is the conductivity depending on the fiber orientation of the plies. The relation between the conductivity and the fiber orientations η is given as

$$\sigma(\eta) = \mathcal{R}(\eta)^\top \cdot \bar{\sigma} \cdot \mathcal{R}(\eta),\tag{42}$$

where $\mathcal{R}(\eta)$ is the rotation matrix,

$$\mathcal{R}(\eta) = \begin{bmatrix} \cos(\eta) & 0 & \sin(\eta) \\ 0 & 1 & 0 \\ -\sin(\eta) & 0 & \cos(\eta) \end{bmatrix}.\tag{43}$$

Here, $\bar{\sigma}$ is a 3×3 constant matrix, which we set as $\bar{\sigma} = \text{diag}(10^{-2}, 10^{-3}, 10^{-3})$. The boundary conditions are given by

$$\begin{aligned}\zeta \cdot n &= 0, \quad \text{on } \partial\mathcal{B} \setminus (\cup E_l), \\ \int_{E_l} \zeta \cdot n dx &= I_l, \quad l = 1, \dots, N_{\text{el}} \\ \frac{1}{E_l} \int_{E_l} u dx + z_l \int_{E_l} \zeta \cdot n dx &= U_l, \quad \text{on } E_l, l = 1, \dots, N_{\text{el}},\end{aligned}\tag{44}$$

where n is the unit outward normal, and I_l and U_l are the applied current and observable electric potential at the electrode E_l , respectively. The first condition states the no-flux condition, while the second one implies that the total injected current through each electrode is known. The third condition captures the surface impedance effect, meaning that the shared interface between the electrode and material has an infinitesimally thin layer with a surface impedance of z_l . In this study, we select $z_l = 0.1$ for the surface impedance. We have the following two constraints (Kirchhoff law of charge conservation and ground potential condition) to guarantee the well-posedness:

$$\sum_{l=1}^{N_{\text{el}}} I_l = 0 \quad \text{and} \quad \sum_{l=1}^{N_{\text{el}}} U_l = 0.\tag{45}$$

6.2 Numerical results

Setting Ten electrodes are placed on the surface of the rectangular domain $\mathcal{B} = [0, 20] \times [0, 2]$, five on the top and five on the bottom. The fiber orientations η_1 in ply \mathcal{B}_1 and η_2 in ply \mathcal{B}_2 are the quantities of interest with the following assumed prior distributions:

$$\eta_1 \sim \mathcal{U}\left(\frac{\pi}{4.5}, \frac{\pi}{3.5}\right), \quad \eta_2 \sim \mathcal{U}\left(-\frac{\pi}{3.5}, -\frac{\pi}{4.5}\right).\tag{46}$$

The observational model is given as

$$\begin{aligned}Y_d &= h(Q, d) + \Xi, \\ \text{where } h(Q, d) &:= [U_1(Q, d), \dots, U_{N_{\text{el}}}(Q, d)]^\top,\end{aligned}\tag{47}$$

and Q is defined in Eq. (40). The observational model h is approximated using the finite element (FE) method. Specifically, we develop a 2D FE model using a quadratic mesh of size 50×6 .

Details on the weak formulation of the FE model are described in Appendix F. We consider two cases of the observational error distribution, $\Xi \sim \mathcal{N}(0, 10^2 \mathbf{I}_{10})$ and $\Xi \sim \mathcal{N}(0, 3^2 \mathbf{I}_{10})$, *i.e.*, the error standard deviations are about 5% and 1.5% of the ground-truth value, respectively. We treat the applied electrode currents as the design parameters denoted as $d := [I_1, \dots, I_{N_{\text{el}}-1}]^\top$, where we enforce that $I_{N_{\text{el}}} = -\sum_{l=1}^{N_{\text{el}}-1} I_l$ in accordance with the Kirchhoff law of charge conservation. We seek the A-optimal DOE parameterized by vector $d \in [-1, 1]^9$.

6.2.1 Error analysis in estimating the tECV

Here we study the errors in estimating the tECV for a specified design parameter vector. For the PACE-based approach, we implement three models: i) using the linear approximation for the CE, see Appendix C.1, ii) using ANN for approximating the CE without data augmentation, and iii) using ANN for approximating the CE and applying the data augmentation method described in Sec. 3.3. The ANNs in cases ii and iii have two hidden layers of 100 neurons. The input and output layers have 10 and 2 neurons, corresponding to the dimensions of vectors y and q , respectively. The dataset D_N is split into two datasets with a size ratio of 1:1 for training and testing, respectively. We use the Adam algorithm [24] with a learning rate of 0.0005 and a batch size of 100. The algorithm is set to run for a maximum of 10000 epochs and features an early-stop mechanism that is activated when the loss function shows no further improvement. To compute the tECV, we fix $M = N$ based on the Proposal 2.

As a closed-form of the tECV is not available in this example, we employ the IS approach with 200000 *i.i.d* samples and use the obtained result as the reference, *i.e.*, the term V in Eq. (26). Fig. 5 depicts the relative MAEs in estimating the tECV for the optimal design found in [17]. To obtain these estimated relative MAEs, we perform 50 statistically independent simulations to empirically compute the expectation operator in Eq. (26).

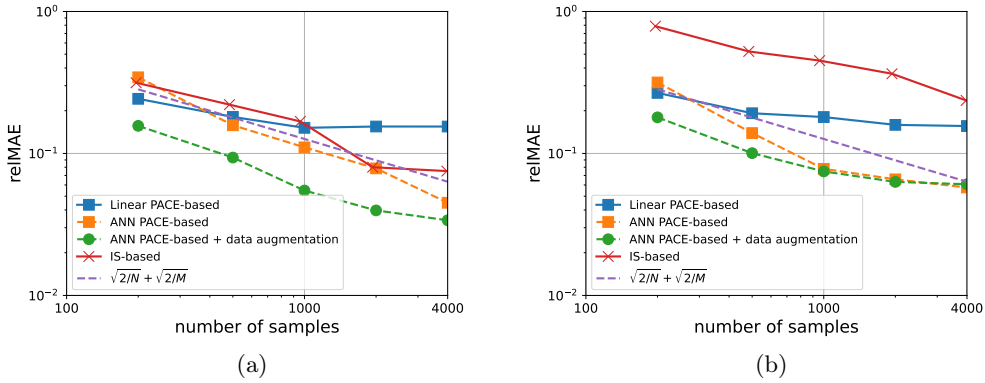


Figure 5: Relative MAE in estimating the tECV for $d = d_{\text{optimal}}$ (a) $\Xi \sim \mathcal{N}(0, 10^2 \mathbf{I}_{10})$, and (b) $\Xi \sim \mathcal{N}(0, 3^2 \mathbf{I}_{10})$. For the PACE-based approach, the numbers of samples equal to $N + M$. For the IS-based approach, the numbers of samples equal to $(N_i + 1) \times N_o$. For the sake of simplicity, we fix $N = M$ and $N_i = N_o$.

Because the measurement map is nonlinear, the bias error of the CE's linear approximation exists and results in a 20% relative MAE of the tCEV. In contrast, we observe negligible bias errors when using ANN for approximating the CE. When comparing models ii and iii, the data augmentation method described in Sec. 3.3 plays a crucial role for reducing the estimating error,

particularly for small numbers of samples, as shown in Fig. 5. For the case $N + M = 200$, applying the data augmentation reduces the relative MAE by more than three times for $\Xi \sim \mathcal{N}(0, 10^2 \mathbf{I}_{10})$.

For the IS-based approach, estimating the tECV requires a double-loop MC simulation, where the numbers of samples of the outer and inner loops are N_o and N_i , respectively, see Appendix A. Here, we set $N_o = N_i$ for simplicity. Optimizing the ratio $N_o : N_i$ is problem dependent and beyond the scope of this work. Compared with the IS-based approach, the PACE-based approach combined with data augmentation significantly decreases the required samples. For example in Fig. 5(a), to reach a relative MAE of 0.9%, the IS approach requires more than 4000 samples. This number is less than 1000 samples in our proposed approach, *i.e.*, more than four times smaller. Notably, for the case $\Xi \sim \mathcal{N}(0, 3^2 \mathbf{I}_{10})$ depicted in Fig. 5(b), while the computational efficiency of the PACE approach does not exhibit a significant change compared with the case in Fig. 5(a), the IS approach performance is sharply reduced. In this case, the IS approach statistical error is even greater than that of the PACE approach using the linear approximation. Moreover, the relative MAE of the PACE approach verifies its theoretical estimation, $\mathcal{O}(\sqrt{\frac{2}{\pi N}} + \sqrt{\frac{2}{\pi M}})$, stated in Proposition 2.

6.2.2 Minimization of the tECV

In this section we apply the algorithms develop in Sec. 5 to determine the A-optimal design of experiment. We approximate the CE non-locally using an ANN of two hidden layers. The input layers have 19 neurons corresponding to the sum of the dimensions of vectors $d \in [-1, 1]^9$ and $y \in \mathbb{R}^{10}$. The number of neurons of the output layer and each hidden layer are two and 100, respectively. We choose the density of the normal distribution $\mathcal{N}(0_9, 0.2 \times \mathbf{I}_9)$ as the kernel function used to evaluate the weighted loss function L_κ in Eq. (36). From this point onward, we keep $\Xi \sim \mathcal{N}(0, 10^2 \mathbf{I}_{10})$ as in [18].

The main procedure described in Algorithm 1 is implemented with 20 iterations. In each iteration, we first use Algorithm 2 to approximate the CE over 1000 epochs. We use $N = 500$ samples to estimate the weighted MSE L_κ , see Eq. (37), and we augment the dataset by 30 times using the data augmentation method described in Sec. 3.3. Other settings for training the ANN are kept identical as in Sec. 6.2.1. Given θ , we execute Algorithm 3 over 20 epochs using $N = 25$ and a single batch. The dataset is also augmented by 30 times. In Algorithm 3, the learning rate is gradually reduced from 0.1 to 0.02 to reduce the stochastic effect in the final epochs, ensuring the algorithm's convergence. Algorithm 3 returns $d_{\kappa+1}$, which is then utilized in the subsequent iteration.

For each iteration of the main procedure, both Algorithm 2 and Algorithm 3 need to evaluate the observational map 500 times. Additionally, the latter evaluates the gradient $\nabla_d h$ 500 more times. In total, Algorithm 1 executes 20000 evaluations of the observational map and 10000 evaluations of the gradient $\nabla_d h$. The total number of evaluations of the observational map and its derivative is only of the same order as estimating the tECV for a single design, see Fig. 5. Our method gains significant computational efficiency owing to the non-local approximation of the CE and the applied transfer learning technique. The performance of the algorithm is depicted in Fig. 6 in terms of the design vector and the tECV. A convergence is clearly observed after 15 iterations.

Optimal designs The A-optimal designs of experiment, found by running the algorithms several times, closely resemble two solutions $d_A = [1, 1, 1, -1, -1, 1, 1, -1, -1]^T$ and $d_A = [-1, -1, -1, 1, 1, -1, -1, 1, 1]^T$, due to the symmetry of the problem. The potential fields solved using the FE model are illustrated in Fig. 7 for the initial guess experimental design and the optimal one. The magnitude of the A-optimal DOE's potential field, particularly at the electrodes, is significantly larger than the initial guess. Consequently, the effect of the measurement error on

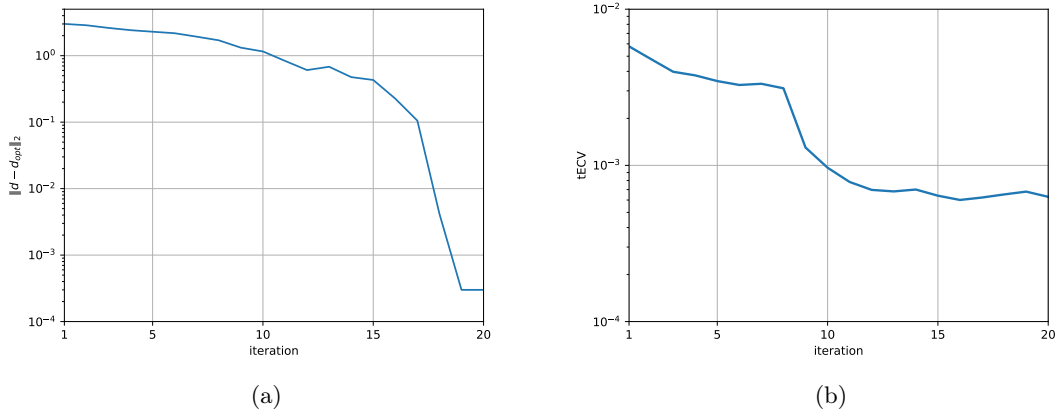


Figure 6: Convergence in terms of the design parameter (a) and the tECV (b).

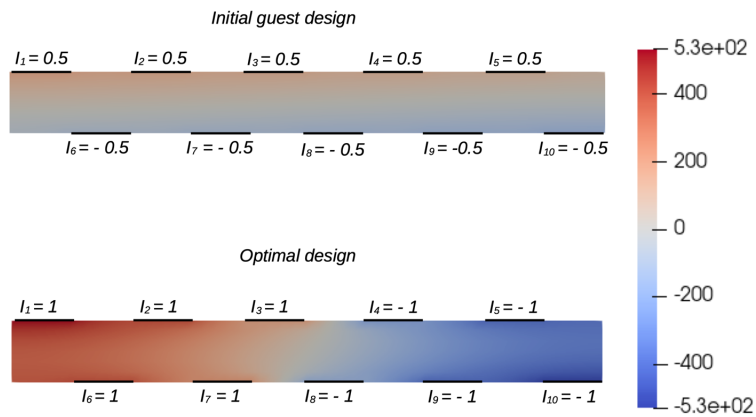


Figure 7: Potential fields solved using the FE model for the initial guess experimental design (above) and the optimal one (below).

the posterior variance is minimized. In this example, minimizing the tECV leads to the optimal designs identical to those that maximize the EIG reported in [18]. This observation suggests that the conditional variance and the information gain are strongly correlated.

Typical posterior densities obtained from the optimal design and the initial guess are depicted in Fig. 8(a) and (b), respectively. The posterior mean inferred using the A-optimal DOE predicts the ground truth value with a negligible error, while the posterior variance is significantly reduced compared with the initial guess design.

7 Conclusion

This work presents an efficient computational method for estimating the tECV within the A-optimal DOE framework using the PACE approach. The intractability of the posterior distribution does not affect the computational efficiency of our approach because both approximating and sampling the posterior distribution are excluded. Moreover, we derive an asymptotical error

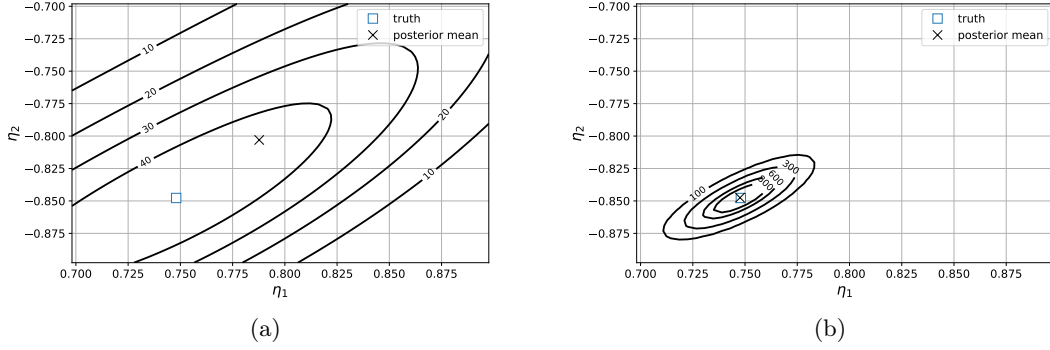


Figure 8: Contour plots of the posterior densities and their mean values for (a) initial DOE and (b) A-optimal DOE. The ground truth value is $\eta_1 = 0.748$, $\eta_2 = -0.848$.

estimation of the method and verify it through numerical experiments.

To address continuous design domains, we combine the PACE framework with stochastic optimization algorithms to seek the A-optimal design of experiments. We demonstrate our method using ANNs to approximate the CE. The stochastic optimization algorithms used for solving the ANN's weights and seeking the optimal design are integrated, as their loss functions are identical. To reduce the number of evaluations of the computationally expensive observation map, we propose a non-local approximation of the CE and apply transfer learning alongside iterative updating of the design candidate. Numerical experiments show that our approach requires significantly fewer evaluations of the observational map compared to the crude importance sampling approach.

A Computing tECV using the IS approach

This appendix describes the computing of the expected conditional variance using the IS estimator of CE. The approach requires a double-loop MC simulation. The inner one is for estimating the posterior variances using Eq. (4), while the outer one is for estimating the expected posterior variance based on Eq. (6).

The outer loop for a given design setting d is formulated as

$$\widehat{V}^{\text{IS}} = \frac{1}{N_o} \sum_{i=1}^{N_o} \sum_{k=1}^n \widehat{\text{Var}}(Q | y^{(i)}), \quad \text{with } y^{(i)} = h(q^{(i)}, d) + \xi^{(i)}, \quad i = 1, \dots, N_o, \quad (48)$$

where $\{q^{(i)}\}_1^{N_o}$ and $\{\xi^{(i)}\}_1^{N_o}$ are N_o *i.i.d.* samples of the RV Q and Ξ , respectively. For each sample pair $(q^{(i)}, y^{(i)})$, an inner loop is performed to estimate the posterior variance as $\widehat{\text{Var}}(Q | y^{(i)})$

$$\widehat{\text{Var}}[Q | y^{(i)}] = \frac{\sum_{j=1}^{N_i} [q^{(i,j)}]^{\odot 2} \pi_{\Xi}(h(q^{(i,j)}, d) - y^{(i)})}{\sum_{j=1}^{N_i} \pi_{\Xi}(h(q^{(i,j)}, d) - y^{(i)})} - \left[\frac{\sum_{j=1}^{N_i} q^{(i,j)} \pi_{\Xi}(h(q^{(i,j)}, d) - y^{(i)})}{\sum_{j=1}^{N_i} \pi_{\Xi}(h(q^{(i,j)}, d) - y^{(i)})} \right]^{\odot 2}, \quad (49)$$

where $\{q^{(i,j)}\}_{i=1, j=1}^{N_o, N_i}$ are $N_i \times N_o$ *i.i.d.* samples of the RV Q . This method requires $(N_i + 1) \times N_o$ evaluations of the observational map h .

B Proofs

B.1 Proof of Proposition 1

Proof. Combining the laws of total mean and total variance of the conditional expectation, *i.e.*

$$\begin{aligned} \mathbb{E}[\mathbb{E}[Q_i | Y_d]] &= \mathbb{E}[Q_i], \\ \text{Var}[Q_i] &= \mathbb{E}[\text{Var}[Q_i | Y_d]] + \text{Var}[\mathbb{E}[Q_i | Y_d]] \end{aligned} \quad (50)$$

for $i = 1, \dots, n$, we attain

$$\mathbb{E}[\text{Var}[Q_i | Y_d]] = \text{Var}[Q_i] - \text{Var}[\mathbb{E}[Q_i | Y_d]] \quad (51)$$

$$= \mathbb{E}[Q_i^2 - \mathbb{E}[Q_i]^2] - \mathbb{E}[\mathbb{E}[Q_i | Y_d]^2 - (\mathbb{E}[\mathbb{E}[Q_i | Y_d]])^2] \quad (52)$$

$$= \mathbb{E}[Q_i^2 - \mathbb{E}[Q_i | Y_d]^2]. \quad (53)$$

Hence, the tECV can be formulated as

$$V(d) \equiv \sum_{i=1}^n \mathbb{E}[\text{Var}[Q_i | Y_d]] \quad (54)$$

$$= \mathbb{E}\left[\sum_{i=1}^n Q_i^2 - \mathbb{E}[Q_i | Y_d]^2\right] \quad (55)$$

$$= \mathbb{E}\left[\|Q - \mathbb{E}[Q | Y_d]\|_2^2\right]. \quad (56)$$

□

B.2 Proof of Proposition 2

Proof. We structure our proof of Proposition 2 in three steps.

Step 1: Estimation of the optimization error ϵ_{opt} . Following the central limit theorem, $\sqrt{N}(\widehat{\mathcal{M}}(f^* | D_N) - \mathcal{M}(f^*)) \rightarrow \mathcal{N}(0, \text{Var}[\|Q - f^*(Y_d)\|_2^2])$ as $N \rightarrow \infty$. For a RV $X \sim \mathcal{N}(0, \sigma^2)$, we have $\mathbb{E}[|X|] = \sqrt{2/\pi} \sigma$. Consequently, the statistical error of the MC estimator $\widehat{\mathcal{M}}(f^* | D_N)$ can be asymptotically estimated as

$$\begin{aligned} \mathbb{E}\left[|\widehat{\mathcal{M}}(f^* | D_N) - \mathcal{M}(f^*)|\right] &\approx \sqrt{\frac{2}{\pi N}} \text{Var}[\|Q - f^*(Y_d)\|_2^2]^{1/2} \\ &= \mathcal{O}\left(\frac{2}{\sqrt{\pi N}} \mathbb{E}\left[\|Q - f^*(Y_d)\|_2^2\right]\right), \end{aligned} \quad (57)$$

where we use the Assumption 2 to obtain the last step. Combining Assumption 3 and the result stated in Eq. (57) yields the following estimation of the optimization error ϵ_{opt}

$$\epsilon_{\text{opt}} = \mathcal{O}\left(\frac{2}{\sqrt{\pi N}} \mathbb{E}\left[\|Q - f^*(Y_d)\|_2^2\right]\right). \quad (58)$$

Moreover, using the orthogonal property $\mathbb{E}[(Q - f^*(Y_d))^\top f(Y_d)] = 0$ for every $f \in \mathcal{S}'$, we have

$$\begin{aligned}
\epsilon_{\text{opt}} &= \mathbb{E} [\|\mathcal{M}(f(\cdot; \boldsymbol{\theta}_{D_N})) - \mathcal{M}(f^*)\|] \\
&= \mathbb{E} \left[\left| \mathbb{E} \left[\|Q - f(Y_d; \boldsymbol{\theta}_{D_N})\|_2^2 \mid \boldsymbol{\theta}_{D_N} \right] - \mathbb{E} \left[\|Q - f^*(Y_d)\|_2^2 \right] \right| \right] \\
&= \mathbb{E} \left[\mathbb{E} \left[\|f(Y_d; \boldsymbol{\theta}_{D_N}) - f^*(Y_d)\|_2^2 \mid \boldsymbol{\theta}_{D_N} \right] \right] \\
&= \mathbb{E} \left[\|f(Y_d; \boldsymbol{\theta}_{D_N}) - f^*(Y_d)\|_2^2 \right].
\end{aligned} \tag{59}$$

Combining Eqs. (58) and (59), we obtain

$$\mathbb{E} \left[\|f(Y_d; \boldsymbol{\theta}_{D_N}) - f^*(Y_d)\|_2^2 \right] = \mathcal{O} \left(\frac{2}{\sqrt{\pi N}} \mathbb{E} \left[\|Q - f^*(Y_d)\|_2^2 \right] \right). \tag{60}$$

Step 2: Estimation of the MC estimator's error ϵ_{MC} . Following central limit theorem, for fixed hyper-parameters $\boldsymbol{\theta}_{D_N}$ as $M \rightarrow \infty$, we have

$$\sqrt{M} \left(\widehat{\mathcal{M}}(f(\cdot; \boldsymbol{\theta}_{D_N}) \mid D_M) - \mathcal{M}(f(Y_d; \boldsymbol{\theta}_{D_N})) \right) \rightarrow \mathcal{N} \left(0, \text{Var} \left[\|Q - f(Y_d; \boldsymbol{\theta}_{D_N})\|_2^2 \mid \boldsymbol{\theta}_{D_N} \right]^{1/2} \right). \tag{61}$$

We estimate the error ϵ_{MC} as $M \rightarrow \infty$ using the central limit theorem as

$$\begin{aligned}
\epsilon_{\text{MC}} &\equiv \mathbb{E} \left[\mathbb{E} \left[\left| \widehat{\mathcal{M}}(f(\cdot; \boldsymbol{\theta}_{D_N}) \mid D_M) - \mathcal{M}(f(Y_d; \boldsymbol{\theta}_{D_N})) \right| \mid \boldsymbol{\theta}_{D_N} \right] \right] \\
&\approx \mathbb{E} \left[\sqrt{\frac{2}{\pi M}} \text{Var} \left[\|Q - f(Y_d; \boldsymbol{\theta}_{D_N})\|_2^2 \mid \boldsymbol{\theta}_{D_N} \right]^{1/2} \right] \\
&= \mathcal{O} \left(\sqrt{\frac{2}{\pi M}} \text{Var} \left[\|Q - f^*(Y_d)\|_2^2 \right]^{1/2} \right) \\
&= \mathcal{O} \left(\frac{2}{\sqrt{\pi M}} \mathbb{E} \left[\|Q - f^*(Y_d)\|_2^2 \right] \right),
\end{aligned} \tag{62}$$

where the third step is obtained owing $\mathbb{E} \left[\|f(Y_d; \boldsymbol{\theta}_{D_N}) - f^*(Y_d)\|_2^2 \right] = \mathcal{O}(2/\sqrt{\pi N})$, obtained from Eq. (60).

Step 3. Eventually, by combining Eqs. (21, 58, 62), we can estimate the error of the estimator $\widehat{V}_d(D_N, D_M)$ as

$$\mathbb{E} \left[\left| \widehat{\mathcal{M}}(f(\cdot; \boldsymbol{\theta}_{D_N}) \mid D_M) - \mathcal{M}(\phi_d) \right| \right] = \mathcal{O} \left(\left(\frac{2}{\sqrt{\pi N}} + \frac{2}{\sqrt{\pi M}} \right) \mathbb{E} \left[\|Q - f^*(Y_d)\|_2^2 \right] \right) + \epsilon_{S'}. \tag{63}$$

□

B.3 Orthogonality property of the CE

Theorem 1 (Orthogonality property). *Let Q and Y be finite-variance RVs valued in \mathbb{R}^n and \mathbb{R}^m , respectively. Let $L_2(\sigma_Y)$ be the collection of all random variables of type $g(Y)$, where $g: \mathbb{R}^m \rightarrow \mathbb{R}^n$ is an arbitrary function satisfying $\mathbb{E} [\|g(Y)\|_2^2] < \infty$. Then,*

$$A) \quad \mathbb{E} \left[f(Y)^\top (Q - \mathbb{E}[Q \mid Y]) \right] = 0, \tag{64}$$

B) the CE $E[Q | Y]$ is the RV in $L_2(\sigma_Y)$ that minimizes the MSE, i.e.,

$$\begin{aligned} E[Q | Y] &= \phi(Y), \\ \text{where } \phi &= \arg \min_{f(Y) \in L_2(\sigma_Y)} E \left[\|Q - f(Y)\|_2^2 \right]. \end{aligned} \quad (65)$$

Proof. For any measurable set $B \subset \mathbb{R}^m$, let $A = Y^f^{-1}(B) \equiv \{\omega : Y(\omega) \in B\}$. As $A \in \sigma_Y$, we achieve

$$\begin{aligned} E[\mathbf{1}_B(Y) (Q - E[Q | Y])] &= E[\mathbf{1}_B(Y) Q] - E[\mathbf{1}_B(Y) E[Q | Y]] \\ &= \int_A Q(\omega) d\mathbb{P}(\omega) - \int_A E[Q | Y](\omega) d\mathbb{P}(\omega) \\ &= 0, \end{aligned} \quad (66)$$

where $\mathbf{1}_B(Y(\omega)) = 1$ if $Y(\omega) \in B$ and 0 otherwise.

Let X^n be a σ_Y -measurable simple RV that converges in terms of distribution to $g \circ Y$. Using the result from Eq. (66), we prove part A).

Let $Z = E[Q | Y] - \phi(Y)$, we have

$$\begin{aligned} E \left[\|Q - \phi(Y)\|_2^2 \right] &= E \left[\|Q - E[Q | Y] + Z\|_2^2 \right] \\ &= E \left[\|Q - E[Q | Y]\|_2^2 \right] + E \left[\|Z\|_2^2 \right], \end{aligned} \quad (67)$$

as the cross-product term vanishes. Eq. (67) straightforwardly shows that

$E \left[\|Q - \phi(Y)\|_2^2 \right]$ is minimized when Z is the n -dimensional vector of zeros, or $E[Q | Y] = \phi(Y)$ (part B). \square

C Linear approximation of the CE

C.1 Analytical formulation of the linear approximation

The linear approximation of the CE, $f_1(Y_d) = \mathbf{A}Y_d + b$, is the solution of the least mean square problem:

$$\mathbf{A}, b = \arg \min_{\mathbf{A}' \in \mathbb{R}^{n \times m}, b' \in \mathbb{R}^n} E \left[\|Q - \mathbf{A}'Y_d - b'\|_2^2 \right]. \quad (68)$$

Using the first order necessary conditions

$$\begin{aligned} E[Q - \mathbf{A}Y_d - b] &= \mathbf{0}_n, \\ E[(Q - \mathbf{A}Y_d - b)Y_d^\top] &= \mathbf{0}_{n \times m}, \end{aligned} \quad (69)$$

where $\mathbf{0}_{n \times m}$ denote the $n \times m$ matrix of zeros, we obtain

$$\begin{aligned} \mathbf{A} &= E \left[(Q - E[Q])Y_d^\top \right] E \left[(Y - E[Y_d])Y^\top \right]^{-1} \\ &= E \left[(Q - E[Q])(Y_d - E[Y_d])^\top \right] E \left[(Y_d - E[Y_d])(Y - E[Y_d])^\top \right]^{-1} \\ &= \text{Cov}[Q, Y_d] \text{Cov}[Y_d]^{-1}, \\ b &= E[Q - \mathbf{A}Y_d]. \end{aligned} \quad (70)$$

C.2 Empirical linear approximation of the CE

Given a dataset $D_N = (q^{(i)}, y^{(i)})_{i=1}^N$ of N *i.i.d.* samples of the RV pair (Q, Y) , the empirical linear approximation of the CE is obtained as

$$\widehat{\phi}(y) = \widehat{\text{Cov}}[Q, Y_d] [\widehat{\text{Cov}}[Y_d]]^{-1} y + \widehat{b} \quad (71)$$

where

$$\begin{aligned} \widehat{\text{Cov}}[Q, Y_d] &= \frac{1}{N} \sum_{i=1}^N [q^{(i)} - \bar{q}] [y^{(i)} - \bar{y}]^\top, \\ \widehat{\text{Cov}}[Y_d, Y_d] &= \frac{1}{N} \sum_{i=1}^N [y^{(i)} - \bar{y}] [y^{(i)} - \bar{y}]^\top, \\ \widehat{b} &= \bar{q} - \frac{1}{N} \sum_{i=1}^N \widehat{\text{Cov}}[Q, Y_d] [\widehat{\text{Cov}}[Y_d]]^{-1} y^{(i)}. \end{aligned} \quad (72)$$

Here, \bar{q} and \bar{y} are empirical means of the RVs Q and Y_d , respectively, computed as

$$\bar{q} = \frac{1}{N} \sum_{i=1}^N q^{(i)}, \quad \bar{y} = \frac{1}{N} \sum_{i=1}^N y^{(i)}. \quad (73)$$

The reduced variance estimators corresponding to those in Eq. (72) are straightforwardly obtained by replacing the role of the dataset D_N with its augmented version D_N^{vr} , see (Eq. 28).

D Reduced variance estimators of MSE and tECV

We show that the estimator $\widehat{\mathcal{M}}^{\text{vr}}$, see Eq. (30), provides an estimation with reduced variance compared with the crude MC one $\widehat{\mathcal{M}}$, see Eq. (16). For a given vector d , we have

$$\begin{aligned} \lim_{a \rightarrow \infty} \widehat{\mathcal{M}}^{\text{vr}}(f | D_N) &=_{\text{a.s.}} \frac{1}{N} \sum_{i=1, \dots, N} \mathbb{E} \left[\left\| q^{(i)} - f(h(q^{(i)}, d) + \Xi) \right\|_2^2 \right] \\ &= \frac{1}{N} \sum_{i=1, \dots, N} \mathbb{E} \left[A(Q, \Xi) | Q = q^{(i)} \right], \end{aligned} \quad (74)$$

\mathbb{P} -almost surely, where

$$A(q, \xi) \equiv \left\| q - f(h(q, d) + \xi) \right\|_2^2. \quad (75)$$

Let $\widehat{\mathcal{M}}^{\text{vr}*}(f)$ denote the right-hand-side term in Eq. (74). Because $\{q^{(i)}\}_{i=1}^N$ are *i.i.d.* samples, we approximately quantify the statistical errors of the estimators $\widehat{\mathcal{M}}$ and $\widehat{\mathcal{M}}^{\text{vr}*}(f)$, respectively, as

$$\text{Var} \left[\widehat{\mathcal{M}}(f | D_N) - \mathbb{E} [A(Q, \Xi)] \right] = \frac{\text{Var} [A(Q, \Xi)]}{N}, \quad (76a)$$

$$\text{Var} \left[\widehat{\mathcal{M}}^{\text{vr}*}(f) - \mathbb{E} [A(Q, \Xi)] \right] = \frac{\text{Var} [\mathbb{E} [A(Q, \Xi) | Q]]}{N}. \quad (76b)$$

Using the law of total variance,

$$\text{Var} [A(Q, \Xi)] = \text{Var} [\mathbb{E} [A(Q, \Xi) | Q]] + \mathbb{E} [\text{Var} [A(Q, \Xi) | Q]], \quad (77)$$

we attain

$$\text{Var} [\mathbb{E} [A(Q, \Xi) | Q]] \leq \text{Var} [A(Q, \Xi)]. \quad (78)$$

Therefore, for $a \gg 1$, $\text{Var} \left[\widehat{\mathcal{M}}^{\text{vr}}(f | D_N) - \mathbb{E} [A(Q, \Xi)] \right] \leq \text{Var} \left[\widehat{\mathcal{M}}(f | D_N) - \mathbb{E} [A(Q, \Xi)] \right]$.

E Gradient of the weighted MSE w.r.t. design parameters

The gradient $\nabla_d \left[\|q - f_N(h(q) + \xi, d)\|_2^2 \right]$ is expanded using the chain rule as

$$\nabla_d \left[\|q - f_N(h(q, d) + \xi, d)\|_2^2 \right] = -2 \left[\nabla_d f_N(y, d) + \nabla_y f_N(y, d) \nabla_d h(q, d) \right]^\top \left[q - f_N(h(q, d) + \xi, d) \right], \quad (79)$$

where $y = h(q, d) + \xi$. Notably, for ANNs f_N , the Jacobian matrices $\nabla_d f_N$ and $\nabla_y f_N$ can be directly obtained numerically using the back-propagation [27]. We finally obtain the value of $\nabla_d \left[\|q - f_N(h(q) + \xi, d)\|_2^2 \right] (q^{(i)}, y^{(i,j)}, d_0)$ as

$$\begin{aligned} \nabla_d \left[\|q - f_N(h(q, d) + \xi, d)\|_2^2 \right] (q^{(i)}, y^{(i,j)}, d_0) = \\ -2 \left[\nabla_d f_N(y^{(i,j)}, d_0) + \nabla_y f_N(y^{(i,j)}, d_0) \nabla_d h(q^{(i)}, d_0) \right]^\top \\ \left[q^{(i)} - f_N(y^{(i,j)}, d_0) \right]. \end{aligned} \quad (80)$$

F Derivation of the finite element formulation

We define $\mathcal{H} := H^1(\mathcal{B} \times \mathbb{R}^{N_{\text{el}}})$ as the space of the solution for the potential field $(u(\omega), U(\omega))$ for $\omega \in \Omega$ and the Bochner space $L_{\mathbb{P}}^2(\Omega; \mathcal{H})$ as

$$L_{\mathbb{P}}^2(\Omega; \mathcal{H}) := \left\{ (u, U) : \Omega \rightarrow \mathcal{H} \quad \text{s.t.} \quad \int_{\Omega} \|(u(\omega), U(\omega))\|_{\mathcal{H}}^2 d\mathbb{P}(\omega) < \infty \right\}, \quad (81)$$

where $U(\omega) = [U_1(\omega), \dots, U_{N_{\text{el}}}(\omega)]^\top$. For the bilinear form $B : \mathcal{H} \times \mathcal{H} \rightarrow \mathbb{R}$, given as

$$B((u, U), (v, V)) := \int_{\mathcal{D}} \sigma \nabla u \cdot \nabla v d\mathcal{B} + \sum_{l=1}^{N_{\text{el}}} \frac{1}{z_l} \int_{E_l} (U_l - u)(V_l - v) dE_l, \quad (82)$$

we aim to determine $(u, U) \in L_{\mathbb{P}}^2(\Omega; \mathcal{H})$ such that the weak formulation

$$B((u(\omega), U(\omega)), (v, V)) = \sum_{l=1}^{N_{\text{el}}} I_l U_l(\omega) \quad (83)$$

is fulfilled for all $(v, V) \in L_{\mathbb{P}}^2(\Omega; \mathcal{H})$ almost surely.

References

- [1] Turab Lookman, Prasanna V Balachandran, Dezhen Xue, and Ruihao Yuan. Active learning in materials science with emphasis on adaptive sampling using uncertainties for targeted design. *npj Computational Materials*, 5(1):21, 2019.
- [2] Laura Ilzarbe, María Jesús Álvarez, Elisabeth Viles, and Martín Tanco. Practical applications of design of experiments in the field of engineering: a bibliographical review. *Quality and Reliability Engineering International*, 24(4):417–428, 2008.

- [3] Stavros N. Politis, Paolo Colombo, Gaia Colombo, and Dimitrios M. Rekkas. Design of experiments (doe) in pharmaceutical development. *Drug development and industrial pharmacy*, 43(6):889–901, 2017.
- [4] Bhupinder Singh, Rajiv Kumar, and Naveen Ahuja. Optimizing drug delivery systems using systematic “design of experiments”. Part I: fundamental aspects. *Critical Reviews™ in Therapeutic Drug Carrier Systems*, 22(1), 2005.
- [5] Roger Mead. *Statistical methods in agriculture and experimental biology*. CRC Press, 2017.
- [6] James H Bullard, Elizabeth Purdom, Kasper D Hansen, and Sandrine Dudoit. Evaluation of statistical methods for normalization and differential expression in mrna-seq experiments. *BMC bioinformatics*, 11(1):1–13, 2010.
- [7] Kathryn Chaloner and Isabella Verdinelli. Bayesian experimental design: A review. *Statistical science*, pages 273–304, 1995.
- [8] Xun Huan and Youssef M. Marzouk. Simulation-based optimal Bayesian experimental design for nonlinear systems. *Journal of Computational Physics*, 232(1):288–317, 2013.
- [9] Alen Alexanderian, Noemi Petra, Georg Stadler, and Omar Ghattas. A-optimal design of experiments for infinite-dimensional Bayesian linear inverse problems with regularized l_0 -sparsification. *SIAM Journal on Scientific Computing*, 36(5):A2122–A2148, 2014.
- [10] Elizabeth G. Ryan, Christopher C. Drovandi, and Anthony N. Pettitt. Simulation-based fully Bayesian experimental design for mixed effects models. *Computational Statistics & Data Analysis*, 92:26–39, 2015.
- [11] Håvard Rue, Sara Martino, and Nicolas Chopin. Approximate bayesian inference for latent gaussian models by using integrated nested laplace approximations. *Journal of the Royal Statistical Society: Series B (Statistical Methodology)*, 71(2):319–392, 2009.
- [12] Elizabeth G. Ryan, Christopher C. Drovandi, James M. McGree, and Anthony N. Pettitt. A review of modern computational algorithms for bayesian optimal design. *International Statistical Review*, 84(1):128–154, 2016.
- [13] Arved Bartuska, Luis Espath, and Raúl Tempone. Small-noise approximation for Bayesian optimal experimental design with nuisance uncertainty. *Computer Methods in Applied Mechanics and Engineering*, 399:115320, 2022.
- [14] Arved Bartuska, André Gustavo Carlon, Luis Espath, Sebastian Krumscheid, and Raúl Tempone. Double-loop quasi-monte carlo estimator for nested integration. *arXiv preprint arXiv:2302.14119*, 2023.
- [15] Alen Alexanderian, Noemi Petra, Georg Stadler, and Omar Ghattas. A fast and scalable method for a-optimal design of experiments for infinite-dimensional Bayesian nonlinear inverse problems. *SIAM Journal on Scientific Computing*, 38(1):A243–A272, 2016.
- [16] Joakim Beck, Ben Mansour Dia, Luis F.R. Espath, Quan Long, and Raúl Tempone. Fast Bayesian experimental design: Laplace-based importance sampling for the expected information gain. *Computer Methods in Applied Mechanics and Engineering*, 334:523–553, 2018.

- [17] Joakim Beck, Ben Mansour Dia, Luis Espath, and Raúl Tempone. Multilevel double loop monte carlo and stochastic collocation methods with importance sampling for Bayesian optimal experimental design. *International Journal for Numerical Methods in Engineering*, 121(15):3482–3503, 2020.
- [18] Nesterov-aided stochastic gradient methods using l.
- [19] Truong-Vinh Hoang, Sebastian Krumscheid, Hermann G. Matthies, and Raúl Tempone. Machine learning-based conditional mean filter: A generalization of the ensemble kalman filter for nonlinear data assimilation. *Foundations of Data Science*, 0:–, 2022.
- [20] Ian Goodfellow, Yoshua Bengio, and Aaron Courville. *Deep learning*. MIT press, 2016.
- [21] Frank Rosenblatt. The perceptron: a probabilistic model for information storage and organization in the brain. *Psychological review*, 65(6):386, 1958.
- [22] Adam Bobrowski. *Functional analysis for Probability and Stochastic Process*. Cambridge University press, 2005.
- [23] Rick Durrett. *Probability: theory and examples*. Cambridge University press, 2019.
- [24] Diederik P. Kingma and Jimmy Ba. Adam: A method for stochastic optimization. *arXiv:1412.6980*, 2014.
- [25] Lisa Torrey and Jude Shavlik. Transfer learning. In *Handbook of research on machine learning applications and trends: algorithms, methods, and techniques*, pages 242–264. IGI global, 2010.
- [26] Karl Weiss, Taghi M Khoshgoftaar, and DingDing Wang. A survey of transfer learning. *Journal of Big data*, 3(1):1–40, 2016.
- [27] Andreas Griewank and Andrea Walther. *Evaluating Derivatives*. Society for Industrial and Applied Mathematics, second edition, 2008.
- [28] Erkki Somersalo, Margaret Cheney, and David Isaacson. Existence and uniqueness for electrode models for electric current computed tomography. *SIAM Journal on Applied Mathematics*, 52(4):1023–1040, 1992.